

# Mechanics of fire ant aggregations

Michael Tennenbaum<sup>1</sup>, Zhongyang Liu<sup>2</sup>, David Hu<sup>2\*</sup> and Alberto Fernandez-Nieves<sup>1</sup>

**Fire ants link their bodies to form aggregations; these can adopt a variety of structures<sup>1–4</sup>, they can drip<sup>2</sup> and spread<sup>4</sup>, or withstand applied loads<sup>5,6</sup>. Here, by using oscillatory rheology, we show that fire ant aggregations are viscoelastic. We find that, at the lowest ant densities probed and in the linear regime, the elastic and viscous moduli are essentially identical over the spanned frequency range, which highlights the absence of a dominant mode of structural relaxation<sup>7</sup>. As ant density increases, the elastic modulus rises, which we interpret by alluding to ant crowding and subsequent jamming. When deformed beyond the linear regime, the aggregation flows, exhibiting shear-thinning behaviour with a stress load that is comparable to the maximum load the aggregation can withstand before individual ants are torn apart. Our findings illustrate the rich, collective mechanical behaviour that can arise in aggregations of active, interacting building blocks.**

Our fire ant aggregations are composed of only workers (Fig. 1a); we selectively leave out the males, eggs and the queen of the colony. The average ant size and mass are  $l \approx 2$  mm and  $m \approx 1.3$  mg, respectively. They are directly extracted from the ground and, before each experiment, they are introduced into a container, which we gently shake to force the ants into close contact<sup>4</sup>. The resulting aggregation clearly exhibits elastic behaviour; when deformed externally by the application of a stress, it returns to essentially its original shape, as shown in Fig. 1b–d and Supplementary Video 1. It also exhibits viscous behaviour; a lead sphere is able to sink through the aggregation very much like a solid object sinks inside a viscous liquid, as shown in Fig. 1e–g and Supplementary Video 2. In which case we can use the measured speed,  $u$ , and the densities of the sphere,  $\rho_{\text{sp}}$ , and the ant aggregation,  $\rho$ , to estimate a viscosity from the balance of the net gravitational force and Stokes drag:  $\eta \approx (\rho_{\text{sp}} - \rho)gr^2/u \approx 35,800$  Pa s, where  $g$  is the acceleration of gravity and  $r$  is the sphere radius. This viscosity corresponds to a shear rate  $u/r \approx 1.9 \times 10^{-3}$  s<sup>-1</sup>. We note that our viscosity estimate is strictly valid for spheres falling through an unbounded simple liquid; corrections due to fluid viscoelastic and wall effects, however, do not appreciably change our result<sup>8</sup>.

To more quantitatively study the mechanics of fire ant aggregations, we use rheology. We employ a stress-controlled rheometer (Anton Paar MCR 501) and a plate–plate geometry. The plates are coated with Velcro to guarantee the no-slip boundary condition; because the mean free path of an ant in the aggregation is comparable to or less than the ant length and the ants entangle and grab the Velcro with a force that is approximately 100 times their body weight, this is a reasonable assumption. The plate diameter is 50 mm and the gap height is set to 3 mm (Supplementary Fig. 1). We have also done experiments with a gap height of 4.5 mm, finding no significant difference with respect to those done at the smaller gap height. For larger gaps, however, gravity causes the ant density to decrease with height, further resulting in the aggregation losing contact with the upper plate. We also use a cylindrical containment

cell to prevent the ants from leaving the region between the plates. Used in this way, the torque above which we are sensitive to the ant aggregation properties is  $\sim 100$   $\mu\text{N m}$ . We always operate above this minimum torque and fix the ant density in our initial experiments to  $\rho = 0.34$  g cm<sup>-3</sup>, corresponding to an effective volume fraction  $\phi_{\text{eff}} = \rho V/m = 1.1$ , where  $V = \pi l^3/6$  is the volume of a sphere with diameter equal to the ant length. This value of  $\phi_{\text{eff}}$  is above random close packing, indicating that the ants are interpenetrating with each other.

We begin by performing controlled shear rate experiments, where we apply a strain rate and measure the stress that is required to maintain the imposed flow. We find that as the shear rate,  $\dot{\gamma}$ , is increased, the stress,  $\sigma$ , also increases. However, within a relatively large range of  $\dot{\gamma}$ , from  $10^{-3}$  s<sup>-1</sup> to  $10^1$  s<sup>-1</sup>, the stress in the sample remains approximately constant and equal to  $\sigma_0 = 70$  Pa = 700 dynes cm<sup>-2</sup>, as shown in Fig. 2a. As a result, the sample viscosity,  $\eta = \sigma/\dot{\gamma}$ , decreases markedly with increasing  $\dot{\gamma}$ . Hence, the ant aggregation shear thins sharply with increasing shear rate, as shown by the squares in Fig. 2b. Indeed, for  $\dot{\gamma} \in [10^{-3}, 10^1]$  s<sup>-1</sup>, we obtain  $\eta \sim \dot{\gamma}^{-1}$ . We note that, in this experiment, we progressively decreased  $\dot{\gamma}$  from  $10^2$  s<sup>-1</sup> to  $10^{-4}$  s<sup>-1</sup>. Similar results are obtained for a different ant aggregation with the same  $\rho$ , but that is subjected to an increasing  $\dot{\gamma}$  from  $10^{-4}$  s<sup>-1</sup> to  $10^2$  s<sup>-1</sup>, as shown by the circles in Fig. 2b. Only at the highest  $\dot{\gamma}$ , for the experiment where we decrease  $\dot{\gamma}$ , and the lowest  $\dot{\gamma}$ , for the experiment where we increase  $\dot{\gamma}$ , do we observe any significant difference between the two situations. In these cases,  $\eta$  does not decrease with  $\dot{\gamma}$ , but rather remains approximately constant. Note that the viscosity obtained from the falling sphere experiment, shown in Fig. 2b with a star, agrees with the viscosity obtained in the controlled shear rate experiment.

To rationalize these results, we consider the dissipation rate per unit volume,  $\Phi \approx \eta \dot{\gamma}^2$ , which, after considering the constitutive law found experimentally,  $\eta = \sigma_0/\dot{\gamma}$ , results in  $\Phi \approx \sigma_0 \dot{\gamma}$ . Note that  $\sigma_0$  is thus an energy loss per unit volume. Interestingly, experiments with dead ants reveal that the viscosity of dead and live ants is identical, as shown in Fig. 2b; when forced to flow, live ants seem to ‘play dead’, ceasing all active motion. We then hypothesize that the energy loss is caused by the friction in the leg joints of the ants; this friction must be overcome for an ant leg to give way and allow strain-rate-induced rearrangements within the aggregation. Indeed, highly frictional joints are a hallmark of insect systems such as stick insects<sup>9</sup>. To confirm our hypothesis, we take a dead ant and remove all but one of its legs. We then bring the ant with its leg oriented perpendicularly to the plate of an analytical balance and measure the force required for the leg to displace itself along the plate a distance  $L \approx 1$  mm, which corresponds to the full range of motion of the leg. We do this while video recording the process. We average  $N = 6$  measurements and obtain a force  $F = (2 \pm 1)$  dynes, corresponding to  $\sim 2$  ant body weights. Considering that an ant has six legs, the energy loss at the joints per volume due

<sup>1</sup>School of Physics, Georgia Institute of Technology, Atlanta, Georgia 30332, USA. <sup>2</sup>School of Mechanical Engineering, Georgia Institute of Technology, Atlanta, Georgia 30332, USA. \*e-mail: hu@me.gatech.edu

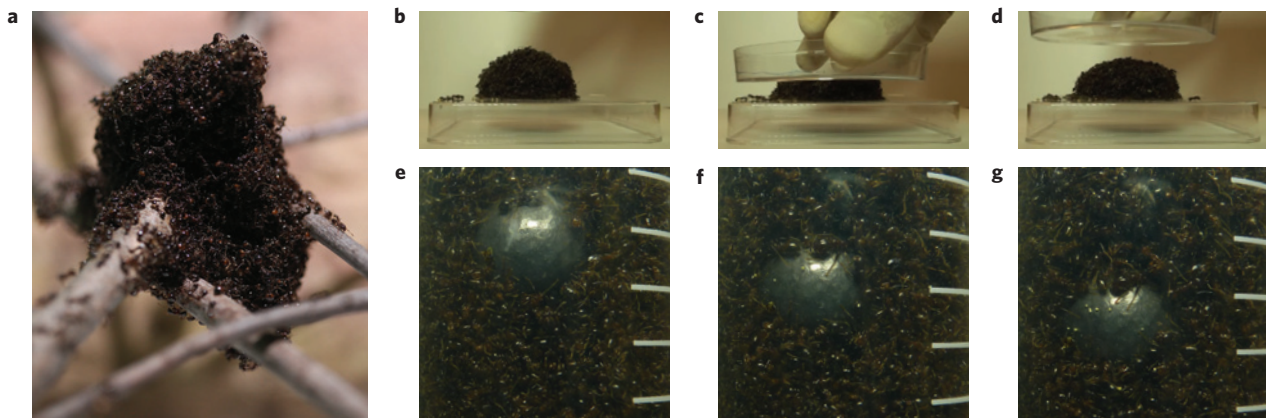


**Figure 1 | Liquid-like and solid-like behaviour of fire ant aggregations.** **a**, A fire ant aggregation composed of workers sitting on sticks. **b–d**, A Petri dish compresses an ant aggregation, which is then left unperturbed. The time lapse between images is 0.2 s. This experiment exemplifies the elastic nature of the ant aggregation in two ways: the aggregation approximately returns to its original shape after being compressed and the aggregation maintains a specific shape. **e–g**, A lead sphere of diameter, 1.1 cm, and density  $\rho_{\text{sp}} \approx 11 \text{ g cm}^{-3}$ , is placed on top of an ant aggregation  $\rho \approx 0.3 \text{ g cm}^{-3}$ , inside a test tube. The test tube is vertical and gravitational acceleration is  $g \approx 10^3 \text{ cm s}^{-2}$ . As time passes, the sphere falls through the aggregation. The time lapse between images is 90 s. The ants flow around the sphere, allowing it to fall at a speed  $u \approx 2 \times 10^{-3} \text{ cm s}^{-1}$ , exemplifying the viscous nature of the ant aggregation at sufficiently long times.

to bending is  $E = 6FL/l^3 \approx 120 \pm 60 \text{ dynes cm}^{-2}$ . This measurement of the energy loss per unit volume is of the same order as the value  $\sigma_0$  found through rheology, indicating that the value of  $\sigma_0$  is associated with the energy required to overcome the friction in the leg joints of the ants. This picture is consistent with a single value of  $\sigma_0$  corresponding to both live and dead ants and suggests that live ants, when forced to flow, indeed ‘play dead’ by allowing their limbs to deform as they would if the ants were dead and lacked inherent activity. The linear dependence of the energy dissipation per unit volume per unit time with  $\dot{\gamma}$  then reflects that the number of joints that deform per unit time also increases linearly with  $\dot{\gamma}$ , a requirement of the shear-thinning behaviour observed experimentally.

To further investigate the flow behaviour of the ant aggregation, we perform creep experiments where we apply a constant stress and measure the time evolution of the strain,  $\gamma$ . Unlike in controlled shear rate experiments, the material is not forced to flow but rather is allowed to spontaneously respond to the applied stress. Interestingly, we observe that the ant aggregation does not flow like a simple liquid. Instead, the strain exhibits regions that are linear with time and regions where the strain remains essentially constant, as shown in Fig. 3a,b for  $\sigma = 40 \text{ Pa}$  and  $\sigma = 70 \text{ Pa}$ , respectively; this implies that the ants dynamically rearrange in response to the applied stress and are even able to store elastic energy over a certain time frame, preventing flow from occurring. We have confirmed that this behaviour is indeed related to the ant activity, by performing creep experiments with dead ant aggregations; in these situations, the strain is a strictly monotonic function of time, as shown in the inset of Fig. 3a, confirming that the intermittent behaviour observed with live ants is indeed due to ant activity. However, the duration of the observed resistance to flow in the case of live ant aggregations decreases with increasing applied stress and eventually, for sufficiently large stresses, it results in a linearly increasing strain and hence a constant shear rate, as shown in Fig. 3c,d. At stresses above  $\sim 250 \text{ Pa}$ , we find that, after the experiment, there are large numbers of ants that have been torn apart; this suggests that the maximum stress the fire ant aggregation can withstand is of this order. Remarkably, this value is not far from  $\sigma_0$ , reflecting that the viscosity of the ant aggregation changes to maintain a constant stress value that is close to the maximum stress the ant aggregation can withstand before individual ants are torn apart. From the linear regions in the strain–time curves, we can determine a shear rate, and

hence a viscosity, which agrees well with the viscosities measured in the controlled shear rate experiments, as shown by the triangles in Fig. 2b. It is worth noting, however, that the flow behaviour in response to the smallest stresses we apply is more complex than the flow behaviour of simple liquids. Nevertheless, the viscosity extracted from the flowing regions agrees with the viscosity we determine when the aggregation is forced to flow at a constant  $\dot{\gamma}$ .

The intriguing flow behaviour for low applied stresses suggests an interesting low-strain behaviour of the ant aggregation, where both energy is stored and dissipated by the material. To test this expectation, we perform oscillatory rheology in the linear regime. In this type of experiment, we apply an oscillatory strain,  $\gamma = \gamma_0 \sin(\omega t)$ , with  $\gamma_0$  the strain amplitude and  $\omega$  the angular frequency, and measure the resultant time dependence of the stress. The strain and stress in a typical cycle for  $\rho = 0.34 \text{ g cm}^{-3}$  and experimental parameters  $\gamma_0 = 0.01$  and  $\omega = 1 \text{ rad s}^{-1}$  is shown in Fig. 4a. Note that the stress is also harmonic. However, it has an in-phase and an out-of-phase component with respect to the applied stress,  $\sigma = \sigma' \sin(\omega t) + \sigma'' \cos(\omega t)$ . This indicates the sample both stores and dissipates energy, consistent with our expectations. The significance of each of these aspects is usually expressed in terms of the elastic or storage modulus,  $G' = \sigma'/\gamma_0$ , and the viscous or dissipative modulus,  $G'' = \sigma''/\gamma_0$ . To identify the linear regime, wherein both shear moduli are independent of the strain amplitude, we fix the frequency to  $1 \text{ rad s}^{-1}$  and perform oscillatory experiments with increasing  $\gamma_0$ . We find that, for  $\rho = 0.34 \text{ g cm}^{-3}$ , the linear regime is approximately fulfilled below  $\gamma_0 \approx 0.04$ , as shown in Fig. 4b. Above this strain amplitude, both moduli decrease with  $\gamma_0$ , reflecting the onset of the nonlinear regime. We then vary the frequency at a fixed  $\gamma_0 = 0.01$ . Remarkably, we find that  $G' \approx G''$  throughout the frequency range we are able to span experimentally, as shown by the black squares in Fig. 4c. This reflects that the ant aggregation is viscoelastic and that the ants are equally dissipating and storing energy. This is markedly different from the behaviour observed for other active materials. For example, flocks of birds and fishes are unable to support applied forces, and so simply flow in response to external perturbations<sup>10,11</sup>. In this case, the birds or the fish are not able to link to each other, but instead are always separated from one another. From this perspective, cell aggregations<sup>12,13</sup> or active liquid crystalline materials<sup>14,15</sup> could be thought of being closer in behaviour to our ant aggregations, because their constituent building blocks are in direct contact

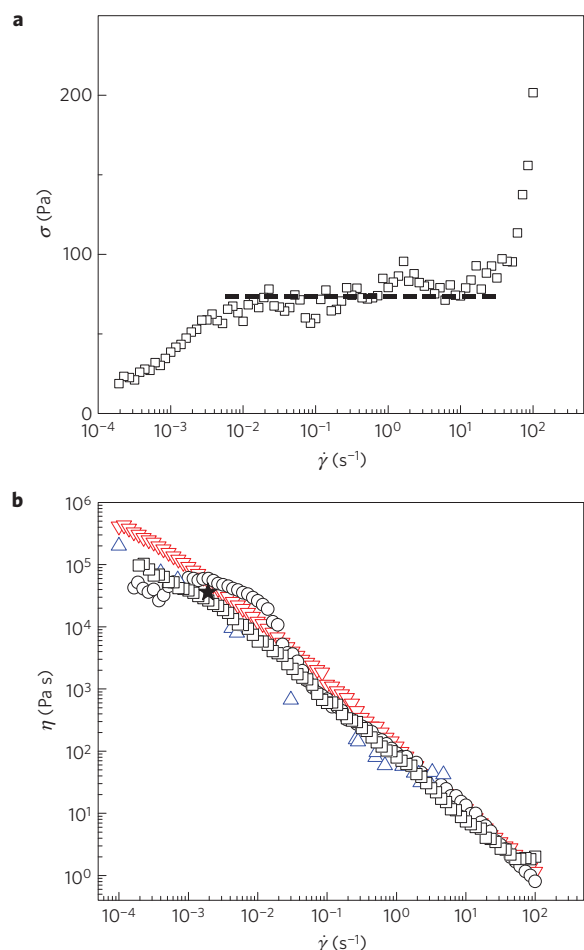


**Figure 2 | Shear thinning of fire ant aggregations.** **a**, Shear stress,  $\sigma$ , as a function of applied shear rate,  $\dot{\gamma}$ . This experiment was done by progressively decreasing the shear rate from  $\sim 10^2 \text{ s}^{-1}$ . For most of the  $\dot{\gamma}$ -range, the ants flow to maintain a constant stress of  $\sim 70 \text{ Pa}$  (indicated by the black dashed line). **b**, Viscosity,  $\eta$ , as a function of shear rate. The squares indicate the viscosities that result by dividing the stress and the shear rate shown in **a**. The circles correspond to a similar experiment where the shear rate is progressively increased from  $2 \times 10^{-4} \text{ s}^{-1}$ . The triangles correspond to viscosities taken from creep experiments where a stress is applied and the strain is measured as a function of time. From the linear parts of these curves, we extract a shear rate, which we can convert into a viscosity by using the value of the applied stress. The black star is the viscosity from the falling sphere in Fig. 1e–g. The ant density in all these experiments is  $0.34 \text{ g cm}^{-3}$ .

with each other and also have the capability to reorganize and assemble into a wide variety of structures. However, once formed, cell assemblies are predominantly elastic, with little or no liquid-like response, and active liquid crystals seem predominantly viscous, with very weak solid-like response. In contrast, we find that fire ant aggregations are characterized by equally important viscous-like and solid-like responses.

A further striking feature of the frequency dependence of the shear moduli is that both  $G'$  and  $G''$  scale with frequency as a power law:  $G' \approx G'' \sim \omega^n$ , with  $n = 0.39 \pm 0.10$ . This is very different from what one observes for a material with a single relaxation time, as shown in Fig. 4d. In this case, the crossover between  $G'$  and  $G''$  occurs at a frequency reflecting the structural relaxation time,  $\tau$ , of the material. For  $t > \tau$ , the material flows like a simple liquid, whereas for  $t \ll \tau$  the material responds elastically. In contrast, the ant aggregation is characterized by a  $G'$  that is

essentially equal to  $G''$  at all accessible frequencies, which can be thought of reflecting the existence of many different relaxation mechanisms in the material. However, we emphasize we cannot rule out the existence of a crossover between  $G'$  and  $G''$ , reflective of a long-time structural relaxation, at a frequency below those we are able to probe in our experiments. We thus conclude that fire ant aggregations have many possible ways to relax stress and dissipate energy, ultimately reflecting their inherent activity and their out-of-equilibrium nature. Real-space imaging indeed reveals that ant aggregations exhibit a wide variety of relaxation mechanisms at different timescales: they constantly change the number of attachments with nearest neighbours, perform internal body motions and experience centre-of-mass motion involving rearrangements with nearest neighbours as well as collective rearrangements (see Supplementary Video 3).

More quantitatively, we can rationalize our result in the context of linear response theory with the Kramers–Kronig relation<sup>16</sup>, which links the in-phase and out-of-phase components of a response function in the frequency domain. This connection is a result of causality and the physical impossibility of responding to a stress before the stress is actually applied<sup>17</sup>. In this case, if both  $G'$  or  $G''$  are power-law functions of the frequency, then both power-law exponents must be equal and  $G' = G'' / \tan(n\pi/2)$ , where  $n$  is the power-law exponent<sup>18</sup>. The ratio of  $G'$  to  $G''$  then provides an alternative way to calculate  $n$ . We do this point-by-point with the oscillatory data for  $\rho = 0.34 \text{ g cm}^{-3}$  and obtain an average of  $n = 0.54 \pm 0.12$ , which is consistent with the result obtained from the fits of  $G'$  and  $G''$  with frequency. Furthermore, because in our experiments  $G' \approx G''$ , indicating congruence, the Kramers–Kronig relations require  $n = 0.5$ , consistent also with what we find experimentally.

Interestingly, the observed power-law behaviour is reminiscent of what is seen for colloidal gels, which consist of small Brownian particles in a solvent that are in constant thermal motion, experiencing random collisions with the surrounding solvent molecules. In the presence of attractive forces and at high enough concentration, the particles aggregate and eventually percolate through the sample, resulting in a kinetically arrested colloidal gel. Near the gelation point, the elastic and viscous moduli can both exhibit power-law behaviour with frequency<sup>19</sup>. This is also seen for polymer gels, where at the critical gelation point both moduli can also be comparable in magnitude<sup>20–22</sup>, similar to what we observe for our ant aggregation. However, although the power-law behaviour of polymer gels at the critical point can be traced back to the fractal structure of the system<sup>7</sup>, real-space analysis of two-dimensional ant aggregations, as well as of frozen three-dimensional aggregations of live ants analysed using microscale computed tomography<sup>5</sup>, suggest that the structure of these materials is not fractal.

The observed congruence of the moduli is progressively lost as  $\rho$  increases, and eventually results in an ant aggregation that is predominantly elastic, as shown in Fig. 4c. For  $\rho = 1.36 \text{ g cm}^{-3}$ , corresponding to an effective volume fraction  $\phi_{\text{eff}} = 4.4$ , the elastic modulus  $G' > G''$  and  $G'$  is weakly dependent on frequency. The power-law behaviour observed at the lowest ant densities within the frequency range probed in our experiments is not maintained at higher densities and the ants are unable to relax as much, hence exhibiting a predominantly elastic behaviour. Note also that the values of  $G'$  increase significantly with  $\rho$ , indicating that the ant aggregation stiffens with increasing density. To quantify this, we correlate elastic modulus with  $\phi_{\text{eff}}$  at a fixed frequency of  $10 \text{ rad s}^{-1}$ ; similar results are obtained at any other frequency. We find that  $G'$  scales linearly with  $\phi_{\text{eff}}$  up to  $\phi_{\text{eff}} \approx 1.4$ , as shown in Fig. 5a. This linear behaviour is also observed in thermal systems such as colloidal hard sphere suspensions or Brownian emulsions in the supercooled liquid regime, below the volume fraction where a colloidal glass forms<sup>23</sup>. In these materials, the elasticity is entropic in nature and arises from

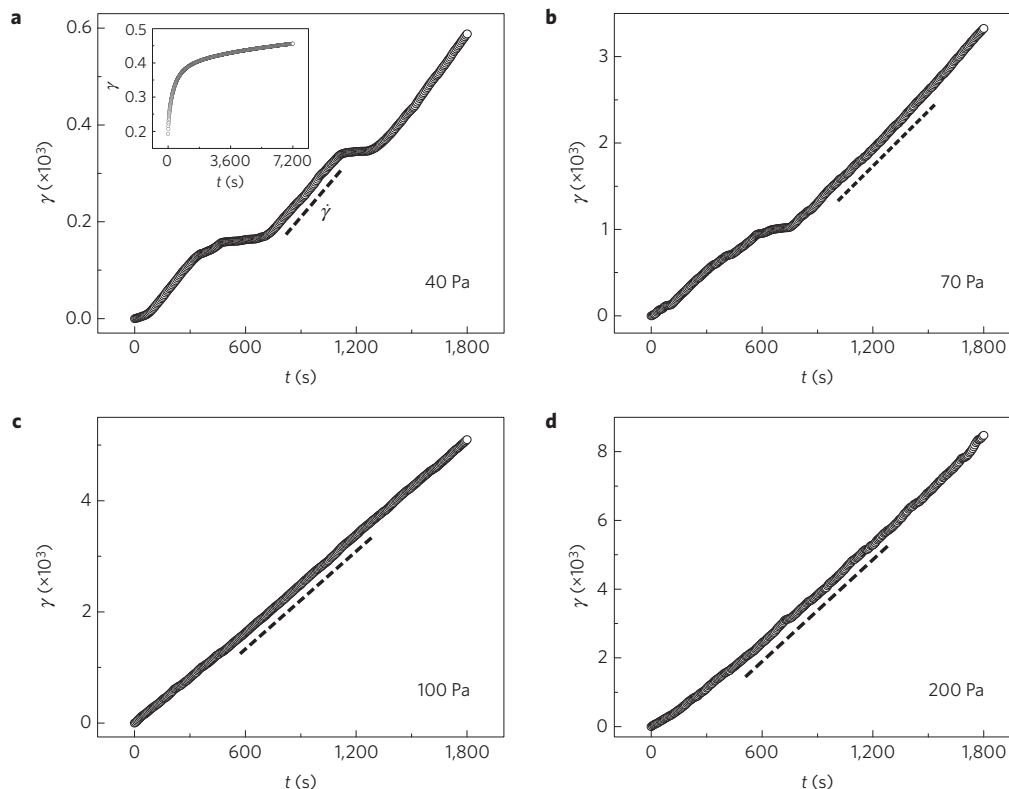


**Figure 3 | Creep behaviour of fire ant aggregations.** Creep experiments of live ants at  $0.34 \text{ g cm}^{-3}$ . For each experiment a fresh aggregation is used. In each test, a step stress, **a**, 40 Pa, **b**, 70 Pa, **c**, 100 Pa, and **d**, 200 Pa, is applied and the strain,  $\gamma$ , is measured as a function of time,  $t$ , for 30 min. In **c, d** the strain is linear throughout the entire experiment, giving a global shear rate. From this and the applied stress we calculate a viscosity:  $\eta = \sigma/\dot{\gamma}$ . In **a, b** there are periods of time when the ants resist the applied stress and times when they flow with it. It is possible, however, to describe a local shear rate in the regions where the strain is linear with time, as illustrated by the dashed line. From the local shear rate we calculate a viscosity. The inset in **a** shows a creep experiment done with a dead ant aggregation at  $0.34 \text{ g cm}^{-3}$  and 40 Pa. The timescale of this test is 2 h, four times longer than the creep experiments with live ant aggregations.

the progressive decrease in the available particle configurations as the particle volume fraction is increased, implying that  $G' \sim kT/a^3$ , with  $k$  the Boltzmann constant,  $T$  the absolute temperature and  $a$  the inter-particle distance. Using  $\rho/m \sim 1/a^3$ , we obtain that  $G'$  scales linearly with volume fraction. We then interpret the linearity of  $G'$  with  $\phi_{\text{eff}}$  below  $\phi_{\text{eff}} \approx 1.4$  for our ant aggregations as resulting from crowding effects and a progressive decrease in the accessible ant configurations with increasing  $\phi_{\text{eff}}$ .

For  $\phi_{\text{eff}} > 1.4$ , this linear behaviour is lost and a new mechanism must now control the elasticity of the ant aggregation. To support this interpretation, we consider a cylindrical volume per ant with length equal to the ant length,  $l$ , and width,  $w_1$ , and obtain  $w_1$  from the condition that these cylinders fill space at  $\phi_{\text{eff}} = 1.4$ . Hence, from the condition  $1 = (\rho/m) [\pi(w_1/2)^2 l]$ , where  $\rho/m$  is obtained from the fact that these cylinders fill space when  $\phi_{\text{eff}} = \rho\pi l^3 / (6m) = 1.4$ , we find  $w_1 = 1.40 \text{ mm}$ . The corresponding cylinder per ant is shown in Fig. 5b, together with an image of a typical ant. Interestingly, the width of the resultant cylinder is close to but slightly smaller than the width of an ant with regularly extended legs. This is then consistent with the idea that below  $\phi_{\text{eff}} = 1.4$  the ants crowd, whereas for  $\phi_{\text{eff}} > 1.4$  a new mechanism, presumably involving leg compression and more direct ant–ant interactions, becomes important. In this new regime,  $G'$  increases faster than linearly with  $\phi_{\text{eff}}$ . The overall behaviour of  $G'$  is described well by  $G' \sim (\phi_c - \phi_{\text{eff}})^{-\alpha}$ , with  $\phi_c = 4.8$  and  $\alpha = 3.5$  (see Fig. 5a). Note that the value of  $\phi_c$  sets the apparent divergence of  $G'$ . Physically, this critical effective volume fraction corresponds to the point where the ants cannot be further compressed. If we again calculate the width of a cylindrical volume associated with an ant, assume that  $1 = (\rho/m) [\pi(w_2/2)^2 l]$  and use

that  $\phi_{\text{eff}} = \phi_c = 4.8$  to obtain  $\rho/m$ , we find  $w_2 = 0.74 \text{ mm}$ , giving the cylinder depicted in Fig. 5c together with an image of a typical ant. Consistent with our interpretation, this width approximately corresponds to the width of an ant body. As a result, if ants were compressed beyond this limit, we would be probing the elasticity of the ant exoskeleton, which has an elastic modulus that is much larger than the elastic modulus of our ant aggregation. Hence, the larger value of this elastic modulus sets the apparent divergence of the elastic modulus of the ant aggregation. Our results thus suggest that the elasticity of the ant aggregation can be understood as resulting from ant crowding first, followed by a jamming transition associated with the compression of the legs of the ants.

In contrast, for dead ants only the weak frequency dependence of the moduli seen at high  $\rho$  for live ants is observed. In these experiments, we freeze a live ant aggregation using liquid nitrogen<sup>5</sup> and subsequently perform the oscillatory shear experiments in the linear regime. We find that, irrespective of the ant density, the elastic modulus  $G' > G''$ , and that it is weakly dependent on frequency, as shown in Fig. 4e. The elastic modulus also increases with ant density. The behaviour of live ants at high  $\rho$  is then reminiscent of that of dead ants, where the importance of dissipation is expected to diminish. Note, however, that we do detect a measurable contribution from  $G''$  in the case of dead ants. We speculate this viscous modulus arises from rearrangements of the ants due their mechanically unstable packing; when loaded in the rheometer, the dead ant aggregation is mechanically unstable, resulting in ant rearrangements. Consistent with this physical picture, the normal force we measure along the span of the oscillatory experiment decreases, indicating that indeed the system is evolving to achieve a mechanically stable packing. Our

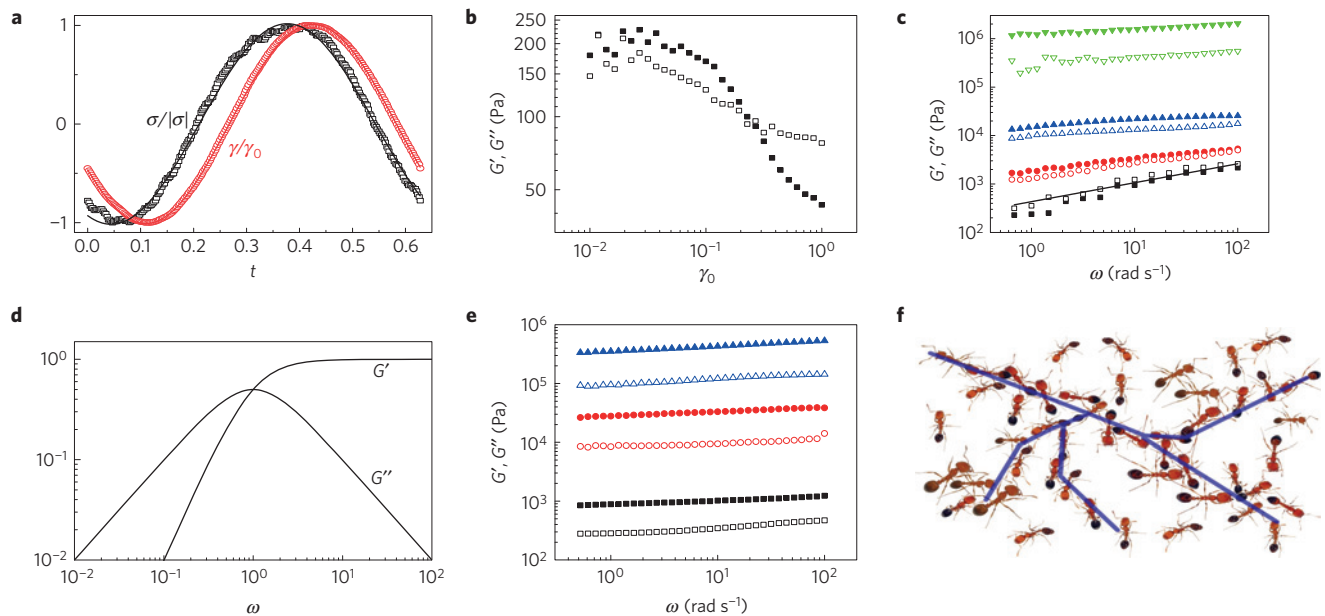


**Figure 4 | Viscoelasticity of fire ant aggregations.** **a**, Waveforms of the applied strain and measured stress from the linear regime of live ants at a density of  $0.34 \text{ g cm}^{-3}$  with the corresponding harmonic fits. They have been normalized with respect to their corresponding amplitudes,  $|\sigma| = \sqrt{\sigma'^2 + \sigma''^2}$  and  $\gamma_0$ . From the fits of the raw waveforms we determine the elastic,  $G'$ , and viscous,  $G''$ , shear moduli. **b**,  $G'$  (filled squares) and  $G''$  (open squares) as a function of strain amplitude,  $\gamma_0$ , for a constant frequency  $\omega = 1 \text{ rad s}^{-1}$  and an ant density of  $0.34 \text{ g cm}^{-3}$ . The cutoff at low-strain amplitude was determined by the minimum torque limit in our experiments. **c**, Frequency sweep in the linear regime for live ants at a density of (squares)  $0.34 \text{ g cm}^{-3}$ , (circles)  $0.68 \text{ g cm}^{-3}$ , (triangles)  $1.02 \text{ g cm}^{-3}$  and (upside-down triangles)  $1.36 \text{ g cm}^{-3}$ .  $G'$  (filled symbols) and  $G''$  (open symbols) are shown. As the ant density is increased the congruence observed for  $\rho = 0.34 \text{ g cm}^{-3}$  disappears, and  $G'$  becomes progressively larger than  $G''$  and more frequency independent. **d**, The simplest model for a viscoelastic material is the so-called Maxwell model<sup>17</sup>, which results from coupling an elastic element and a viscous element in series. The result is a shear rate containing both contributions:  $\dot{\gamma} = \dot{\sigma}/G_0 + \sigma/\eta$ , with  $G_0$  the instantaneous elastic modulus. By applying a sinusoidal strain, we can calculate the stress from this equation, and from here the shear moduli,  $G' = (G_0 \eta^2 \omega^2)/(G_0^2 + \eta^2 \omega^2)$  and  $G'' = (G_0^2 \eta \omega)/(G_0^2 + \eta^2 \omega^2)$ . In this graph, we show the frequency dependence of  $G'$  and  $G''$  with  $G_0 = 1 \text{ Pa}$  and  $\eta = 1 \text{ Pa s}$ . The main feature is the existence of a crossover point between  $G'$  and  $G''$ , indicating there is a single relaxation time for the material. The behaviour seen for ant aggregations differs markedly from the expectations of the Maxwell model, indicating that these materials do not have a single relaxation time within the frequency range probed. **e**, Frequency sweeps of dead ants in the linear regime for ant densities of (squares)  $0.34 \text{ g cm}^{-3}$ , (circles)  $0.68 \text{ g cm}^{-3}$  and (triangles)  $1.02 \text{ g cm}^{-3}$ . For all three densities  $G'$  (filled symbols) is larger than  $G''$  (open symbols) over the entire frequency range and exhibits little frequency dependence. This indicates the elastic nature of the dead ant aggregations. **f**, Schematic of a live ant aggregation. The connectivity between ants results in the elastic nature of the aggregation, whereas the break-up of contacts and ant rearrangements results in the viscous nature of the aggregation. The formation and breaking of these inter-ant contacts is what results in the observed viscoelastic behaviour.

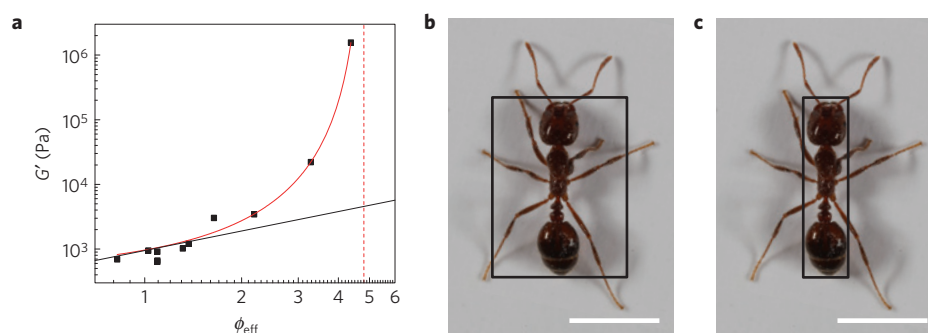


**Figure 5 | Elastic modulus of fire ant aggregations.** **a**, Storage modulus,  $G'$ , as a function of effective volume fraction,  $\phi_{\text{eff}}$ . The black line shows the initial linear scaling of  $G'$ :  $G' \sim \phi_{\text{eff}}$ . After  $\phi_{\text{eff}} = 1.4$ ,  $G'$  begins to increase faster than linearly. This is described by  $G' \sim (\phi_c - \phi_{\text{eff}})^{-\alpha}$ , shown by the red line, with  $\phi_c = 4.8$  and  $\alpha = 3.5$ . The divergence at  $\phi_c = 4.8$  is shown by a red dashed line. **b**, A cylinder of length,  $l = 2 \text{ mm}$ , and width,  $w_1 = 1.40 \text{ mm}$ , overlaid on an ant. The cylinder sits just inside the reach of the ant legs. This corresponds to a  $\phi_{\text{eff}}$  of 1.4, the transition from linear to nonlinear scaling of  $G'$  with  $\phi_{\text{eff}}$ . **c**, A cylinder of length,  $l = 2 \text{ mm}$ , and width,  $w_2 = 0.74 \text{ mm}$ , overlaid on an ant. The cylinder fits closely around the body of the ant. This corresponds to the divergence of  $G'$  shown in **a** at  $\phi_{\text{eff}} = \phi_c = 4.8$ . Scale bars in **b** and **c** are 1 mm.

results in the linear regime clearly indicate that the mechanics of live ant aggregations are characterized by much more ant motion than dead ant aggregations; this is reminiscent of what is seen for active particles compared to Brownian particles<sup>24–27</sup>.

Overall, we have found that fire ants at densities corresponding to effective volume fractions above random close packing move and rearrange and exhibit power-law oscillatory rheology, within the frequency range probed in our experiments. These rearrangements

result in the active break-up and formation of contacts between the ants. However, at a given time instant, the ant aggregation forms a network that spans and percolates throughout the containment cell, as shown schematically in Fig. 4f. Interestingly, the contribution from  $G''$  to the linear viscoelastic response is comparable to the contribution from  $G'$ . Hence, fire ants constantly store and dissipate energy, a fact that they probably actively exploit in nature when maintaining structures such as bridges and towers in unpredictable environments. Interestingly, with increasing ant densities, the aggregation becomes predominantly elastic and increasingly stiffer, a fact that they also exploit in real life for the structures they make to withstand their shape against gravity. This increase in elasticity is consistent with an initial crowding mechanism associated with a decrease in the available ant configurations as  $\phi_{\text{eff}}$  increases. At higher  $\phi_{\text{eff}}$ , jamming occurs when the ants are forced to compress their legs and appreciably interact with their neighbours. Our results illustrate how rich collective mechanical behaviour arises when individual active building blocks come together and interact. In this case, the properties of the collectivity arise from the individual activity. Further theoretical and computational work will aid in understanding how the observed macroscopic behaviour results from the individual ant behaviour. This could in turn provide inspiration in the field of modular robotics<sup>28,29</sup>, whereby complex collective behaviour could result from the simpler motion of small robotic units that could be made to resemble individual ants. In addition, we emphasize that the behaviour observed for the ant aggregation is, in some aspects, reminiscent of the behaviour exhibited by thermal systems. However, whereas for thermal systems the concept of equilibrium is of paramount importance, for active systems such as fire ant aggregations, a framework accounting for the fact that the individual constituents are out-of-equilibrium is required. Similar situations arise within cells, where the role of the cellular motors results in a behaviour that is reminiscent of thermal behaviour<sup>30</sup>. We believe our work is just the beginning of what can be done using fire ants as active materials.

Received 26 September 2014; accepted 17 September 2015;  
published online 26 October 2015

## References

1. Anderson, C., Theraulaz, G. & Deneubourg, J.-L. Self-assemblages in insect societies. *Insect. Soc.* **49**, 99–110 (2002).
2. Bonabeau, E. *et al.* Dripping faucet with ants. *Phys. Rev. E* **57**, 5904–5907 (1998).
3. Hölldobler, B. *The Ants* (Harvard Univ. Press, 1990).
4. Mlot, N. J., Tovey, C. A. & Hu, D. L. Fire ants self-assemble into waterproof rafts to survive floods. *Proc. Natl Acad. Sci. USA* **108**, 7669–7673 (2011).
5. Foster, P. C., Mlot, N. J., Lin, A. & Hu, D. L. Fire ants actively control spacing and orientation within self-assemblages. *J. Exp. Biol.* **217**, 2089–2100 (2014).
6. Schneirla, T. C. *Army Ants: A Study in Social Organization* (W. H. Freeman, 1971).
7. Winter, H. H. & Mours, M. *Neutron Spin Echo Spectroscopy Viscoelasticity Rheology* 165–234 (Springer, 1997).
8. Chhabra, R. P. *Bubbles, Drops, and Particles in Non-Newtonian Fluids* (CRC Press, 2006).
9. Zill, S. N., Chaudhry, S., Büschges, A. & Schmitz, J. Directional specificity and encoding of muscle forces and loads by stick insect tibial campaniform sensilla, including receptors with round cuticular caps. *Arth. Struct. Dev.* **42**, 455–467 (2013).

10. Couzin, I. D. & Krause, J. in *Advances in the Study of Behavior* Vol. 32, 1–75 (Academic Press, 2003).
11. Sumpter, D. J. The principles of collective animal behaviour. *Phil. Trans. R Soc. Lond. B* **361**, 5–22 (2006).
12. Alcaraz, J. *et al.* Microrheology of human lung epithelial cells measured by atomic force microscopy. *Biophys. J.* **84**, 2071–2079 (2003).
13. Gisler, T. & Weitz, D. A. Scaling of the microrheology of semidilute F-actin solutions. *Phys. Rev. Lett.* **82**, 1606 (1999).
14. Marchetti, M. C. Active matter: Spontaneous flows and self-propelled drops. *Nature* **491**, 340–341 (2012).
15. Sanchez, T., Chen, D. T. N., DeCamp, S. J., Heymann, M. & Dogic, Z. Spontaneous motion in hierarchically assembled active matter. *Nature* **491**, 431–434 (2012).
16. Stone, M. & Goldbart, P. *Mathematics for Physics: A Guided Tour for Graduate Students* (Cambridge Univ. Press, 2009).
17. Bird, R. B., Armstrong, R. C. & Hassager, O. *Dynamics of Polymeric Liquids, Fluid Mechanics* 2nd edn (Wiley, 1987).
18. Winter, H. H. & Chambon, F. Analysis of linear viscoelasticity of a crosslinking polymer at the gel point. *J. Rheol.* **30**, 367–382 (1986).
19. Krall, A. H. & Weitz, D. A. Internal dynamics and elasticity of fractal colloidal gels. *Phys. Rev. Lett.* **80**, 778–781 (1998).
20. Fabry, B. *et al.* Scaling the microrheology of living cells. *Phys. Rev. Lett.* **87**, 148102 (2001).
21. Ng, T. S. K. & McKinley, G. H. Power law gels at finite strains: The nonlinear rheology of gluten gels. *J. Rheol.* **52**, 417 (2008).
22. Trappe, V. & Sandkühler, P. Colloidal gels—low-density disordered solid-like states. *Curr. Opin. Colloid Interface Sci.* **8**, 494–500 (2004).
23. Mason, T., Bibette, J. & Weitz, D. Elasticity of compressed emulsions. *Phys. Rev. Lett.* **75**, 2051–2054 (1995).
24. Angelini, T. E. *et al.* Glass-like dynamics of collective cell migration. *Proc. Natl Acad. Sci. USA* **108**, 4714–4719 (2011).
25. Berthier, L. Nonequilibrium glassy dynamics of self-propelled hard disks. *Phys. Rev. Lett.* **112**, 220602 (2014).
26. Gonzalez-Rodriguez, D., Guevorkian, K., Douezan, S. & Brochard-Wyart, F. Soft matter models of developing tissues and tumors. *Science* **338**, 910–917 (2012).
27. Ni, R., Stuart, M. A. C. & Dijkstra, M. Pushing the glass transition towards random close packing using self-propelled hard spheres. *Nature Commun.* **4**, 2704 (2013).
28. Rubenstein, M., Cornejo, A. & Nagpal, R. Programmable self-assembly in a thousand-robot swarm. *Science* **345**, 795–799 (2014).
29. Werfel, J., Petersen, K. & Nagpal, R. Designing collective behavior in a termite-inspired robot construction team. *Science* **343**, 754–758 (2014).
30. Janmey, P. A. & Weitz, D. A. Dealing with mechanics: Mechanisms of force transduction in cells. *Trends Biochem. Sci.* **29**, 364–370 (2004).

## Acknowledgements

This research is supported by the US Army Research Laboratory and the US Army Research Office Mechanical Sciences Division, Complex Dynamics and Systems Program, under contract numbers W911NF-12-R-0011 and W911NF-14-1-0487. We are also grateful to L. Mahadevan and G. McKinley for useful discussions.

## Author contributions

M.T. and Z.L. performed experiments. M.T., D.H. and A.F.-N. designed experiments. M.T., D.H. and A.F.-N. analysed and interpreted data. M.T., D.H. and A.F.-N. wrote the paper.

## Additional information

Supplementary information is available in the [online version of the paper](#). Reprints and permissions information is available online at [www.nature.com/reprints](http://www.nature.com/reprints). Correspondence and requests for materials should be addressed to D.H.

## Competing financial interests

The authors declare no competing financial interests.